Charged-particle–producing reactions of 15-MeV neutrons on ^{51}V and ^{93}Nb†

S. M. Grimes, R. C. Haight, and J. D. Anderson
Lawrence Livermore Laboratory, Livermore, California 94550
(Received 19 July 1977)

Cross sections for the (n,xp), (n,d), and $(n,x\alpha)$ reactions for 15-MeV neutrons on ^{51}V and ^{93}Nb have been measured with a magnetic quadrupole spectrometer. The importance of the $(n,n'p)$ reaction as a source of protons is examined by comparing these results with those recently obtained for ^{46}Ti. Good fits to the (n,xp) and $(n,x\alpha)$ energy spectra require contributions from both equilibrium and nonequilibrium reactions, while only the latter appear in the (n,d) spectra. Calculated values for the $(n,n'p)$ and $(n,n'\alpha)$ cross sections agree well with the experimental values. The cross sections are ^{51}V(n,xp) 91 ± 14 mb, ^{51}V(n,xd) 7 ± 3 mb, ^{51}V$(n,x\alpha)$ 17 ± 3 mb, ^{93}Nb(n,xp) 51 ± 8 mb, ^{93}Nb(n,xd) 8 ± 3 mb, and ^{93}Nb$(n,x\alpha)$ 14 ± 3 mb.

[NUCLEAR REACTIONS ^{51}V(n,xp), ^{51}V(n,xd), ^{51}V$(n,x\alpha)$, ^{93}Nb(n,xp), ^{93}Nb(n,xd), ^{93}Nb$(n,x\alpha)$, $E_n=14.8$ MeV, measured $\sigma(E_p,\theta)$, $\sigma(E_d,\theta)$, $\sigma(E_\alpha,\theta)$, Hauser-Feshbach analysis; deduced reaction mechanism.]

I. INTRODUCTION

A recent measurement[1] of the (n, xp) and $(n, x\alpha)$ spectra for 15-MeV neutrons on Al and Ti has shown that reactions involving sequential nucleon emission can produce large sub-Coulomb-barrier contributions to charged particle spectra. For target nuclei in which the binding energy of the last neutron is greater than that of the last proton, the (n, n') reaction can populate states whose only available decay channels are sub-Coulomb barrier charged particle emission and γ decay. The measurements reported in Ref. 1 suggest that states which can emit protons of 1 MeV or more will decay predominantly by proton decay, while states with less energy available will typically γ decay. Comparison of the proton and α barrier penetrabilities suggested[1] that the corresponding energy for α-particle decay was about 4 MeV for these nuclei. Thus, even though the α binding energy is slightly less than that for protons in these nuclei, the α spectra showed only hints of subbarrier contributions, while the corresponding proton component was a large fraction of the spectrum. Finally, the correspondence of the subbarrier peak to the $(n, n'p)$ reaction was established by comparing the (n, xp) spectra for ^{46}Ti and ^{48}Ti; in the former nucleus, the proton binding energy is less than the neutron binding energy and a large low energy peak was observed, while for ^{48}Ti, the binding energies are nearly equal and no low energy peak was seen.

The present measurements were undertaken to investigate the importance of this mechanism in producing charged particles for other target nuclei. Vanadium and niobium were chosen as targets both because of their potential use as materials in fusion reactors and because in both cases the binding energy relationship was such that a subbarrier proton peak could occur. Complete charged-particle spectra were obtained to enable a comparison of the magnitude of the subbarrier peak with the total charged-particle production cross section. Analysis of the angular and emission energy dependence indicated that compound nuclear processes are an important source of charged particles even for targets as heavy as Nb, although the relative importance of nonequilibrium reaction contributions was considerably greater than for nuclei with $A \lesssim 50$.

Many of the measurements of neutron-induced charged-particle producing cross sections have been made with radiochemical techniques. These measurements are considerably easier than those involving detection of the charged particles since a single measurement yields the cross section for a given reaction channel integrated over the angle and energy distribution of the light charged particle. This technique would not be useful in studying the importance of $(n, n'p)$ reactions however because they populate the same residual nucleus as the (n, d) reaction. In addition, as pointed out in Ref. 1, the $(n, n'p)$ reaction is likely to be of particular importance for targets for which the final nucleus reached by this reaction is stable.

Detection of low energy charged particles resulting from 15 MeV neutron induced reactions is quite difficult. The target must be relatively thin to allow the charged particles to escape and there are generally many sources of low energy charged particles in a neutron environment other than the sample of interest. Measurements presented in

Ref. 1 show that the use of an intense neutron source and a magnetic quadrupole spectrometer allows the detection of protons with energies as low as 1 MeV.

II. EXPERIMENTAL PROCEDURE

A magnetic quadrupole spectrometer was used to detect the charged particles. As has been previously discussed,[1,2] such a spectrometer allows a large neutron source-to-detector separation and thereby reduces the background produced in the detector by neutron or γ-ray-induced reactions. This spectrometer also can discriminate to some degree against charged particles produced at locations other than the radiator of interest. The principal disadvantage of the spectrometer is its energy selectivity, which requires measurements to be made at a number of magnetic field gradient settings in order to obtain the entire spectrum.

Details of the experimental procedure were identical to those described in Ref. 1. The source of neutrons was the rotating-target neutron source at the Lawrence Livermore Laboratory. An intensity of about 3×10^{12} neutrons/sec into 4π sr was used for these measurements.

The spectrometer consists of a magnetic quadrupole doublet lens and the associated reaction chamber, transport tube, and detector telescope. Because the axis of the spectrometer was perpendicular to the beam direction and was 5 cm behind the neutron source, changes in reaction angle could be made by translating the spectrometer along its axis. This changed the angle between the direction of neutrons incident on the target and the outgoing charged particles by moving the radiator foil relative to the neutron source. Such a procedure for changing the reaction angle resulted in a change in the ^{3}H(d, n) neutron production angle and hence a small change in the average neutron energy from 15.1 MeV at $\theta_{^3\mathrm{H}(d,n)}=0°(\theta_{(\mathrm{n,\ charged\ particle})}=90°)$ to 14.8 for $\theta_{^3\mathrm{H}(d,n)}=45°(\theta_{(\mathrm{n,charged\ particle})}=45°)$.

Charged particles were detected in a two-detector counter telescope. A 15-μm thick silicon surface barrier detector served as a ΔE detector, while the E detector was 1500 μm thick. The total energy and particle species were determined with conventional electronics.

The spectrometer acceptance was inferred from measurements of spectra produced by neutron bombardment of stopping targets of CH_2 and CD_2. These radiators produce protons (from CH_2) or deuterons (from CD_2) from elastic n-p or n-d scattering which because of energy losses in the radiator will have energies ranging from $E_n\cos^2\theta$ (protons) or $\frac{8}{9}E_n\cos^2\theta$ (deuterons) to zero energy. The spectral shape can be calculated from the known elastic cross sections and angular distributions and the stopping powers of polyethylene. Comparison of the measured spectral shape with that calculated for a given incident neutron flux yields the acceptance as a function of energy for a given quadrupole current. This calibration was carried out for each quadrupole gradient setting at which data were taken.

In principle, the acceptance of such a spectrometer is a function only of Z^2/ME, which would suggest that the α-particle acceptance could be taken to be identical to that for protons. Because the energy loss in the ΔE detector for high energy protons was only slightly above the electronic bias, some counting loss in the counter telescope occurred for these particles. These losses will occur for the measured spectra as well but will be corrected for by the corresponding reduction in measured acceptance. The pulses for high energy deuterons and α particles were considerably above the electronic cutoff, so the α acceptance function was obtained by shifting the deuteron function to energies twice as large. Use of the deuteron acceptance function to obtain that for α particles has the additional advantage that multiple scattering in the ΔE detector[1] which could cause particles to miss the E detector is almost identical for α particles at E_0 as for deuterons of energy $\frac{1}{2}E_0$.

Energy spectra were obtained at 45, 75, and 135°. Since the purpose of the experiment was to examine the relative importance of (n, $n'p$) and (n, $n'\alpha$) processes in producing charged particles, it was felt to be more important to cover the entire energy spectrum than to make measurements at a large number of angles. For protons and α particles, large fractions of the spectra [including the (n, $n'p$) and (n, $n'\alpha$) portions] are due to compound nuclear processes, for which an isotropic or symmetric angular distribution would be expected. Even for direct or preequilibrium portions of the spectra which would be forward peaked, the three angles chosen should give a better estimate of the total cross section than small angles, because of the reduction in solid angle as the angle approaches 0° or 180°.

The counter telescope could detect protons with energies as low as 1.1 MeV, with corresponding cutoffs for deuterons and α particles of 1.8 and 4.3 MeV, respectively. Use of a single detector instead of the telescope as was described in Ref. 1 was not necessary because the present targets did not produce protons with energies as low as those from aluminum.

III. RESULTS

Raw data at two magnet settings are shown in Figs. 1(a) and 1(b) for the protons emitted at 75°

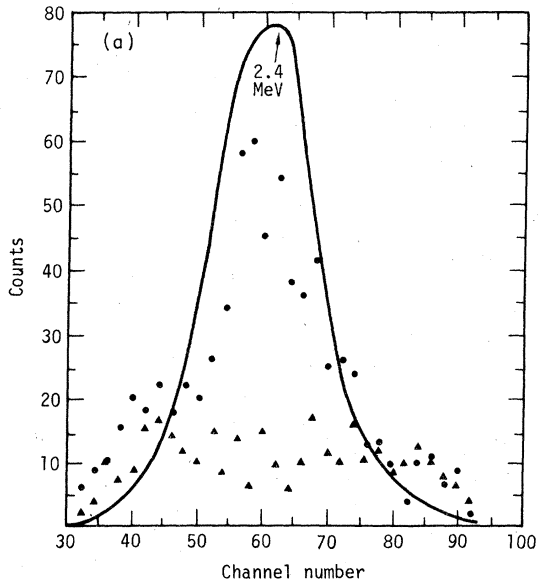

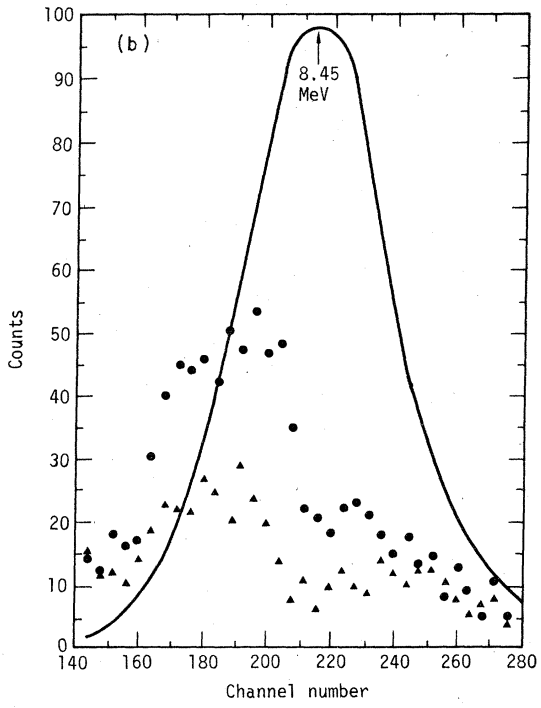

FIG. 1. (a) Spectra for the $^{51}V(n,xp)$ reaction at a magnet setting corresponding to 2.4 MeV protons. The solid circles denote the number of counts (summed over two channels) with the radiator in place; the triangles represent the corresponding number of counts with the radiator removed. The solid line indicates the relative acceptance of the spectrometer as a function of energy. (b) Same as (a), except that the magnet setting corresponds to 8.45-MeV protons.

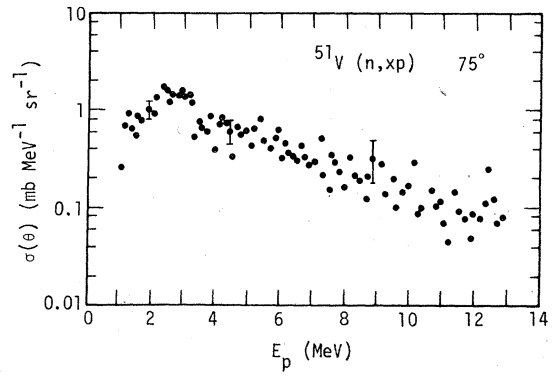

FIG. 2. Spectrum for the $^{51}V(n,xp)$ reaction at 75°. These cross sections are the result of adding together cross sections derived from eight spectra of the type shown in Figs. 1(a) and 1(b).

from ^{51}V under bombardment by 15-MeV neutrons. The spectra with the target foil in are denoted by solid circles and those with the foil out by triangles. Solid curves show the acceptance functions of the spectrometer for the different magnet settings. The complete proton spectrum, made by combining eight pairs of foil-in–foil-out data, is shown in Fig. 2. Representative statistical error bars are shown for three points.

Differential energy spectra for protons, deuter-

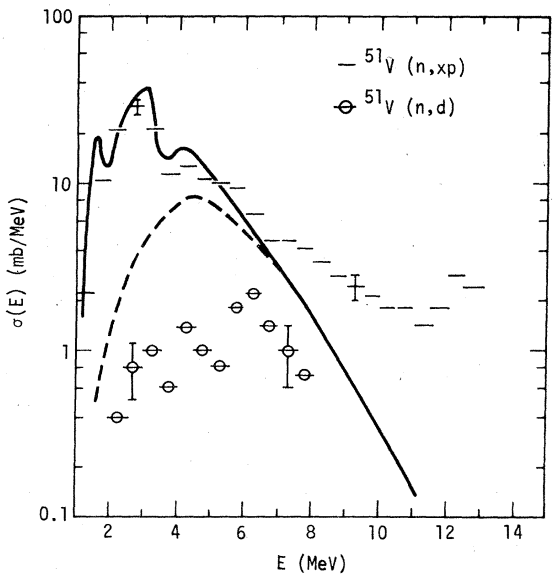

FIG. 3. Angle-integrated spectra for the $^{51}V(n,xp)$ and $^{51}V(n,d)$ reactions. The horizontal lines give the measured cross section for the (n,xp) reaction, while the θ symbol denotes those for the (n,d) reaction. The dashed line gives the spectrum due to proton evaporation from the compound nucleus ^{52}V; the solid line shows the result of adding this to the contribution from protons emitted as the second particle in a two-stage reaction.

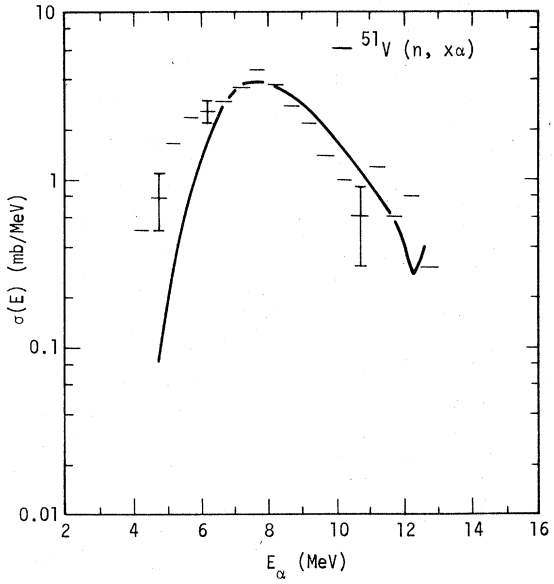

FIG. 4. Angle-integrated spectra for the $^{51}V(n,x\alpha)$ reaction. The solid line represents the result of a Hauser-Feshbach calculation described in the text. For this reaction the predicted second-stage α decay is too small to be observed.

ons, and α particles were summed over 500-keV intervals and then averaged over angle to obtain angle-integrated cross sections in the laboratory system. The resulting cross sections are shown in Figs. 3–6 and the energy-integrated values are given in Table I.

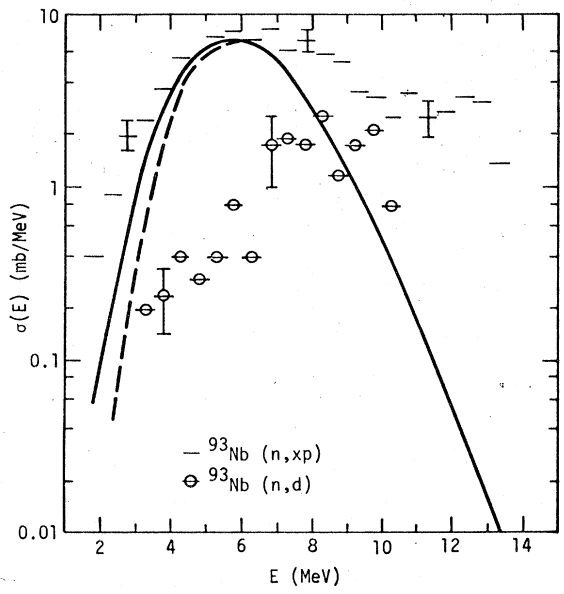

FIG. 5. Same as Fig. 3 for the $^{93}Nb(n,xp)$ and $^{93}Nb(n,d)$ reactions.

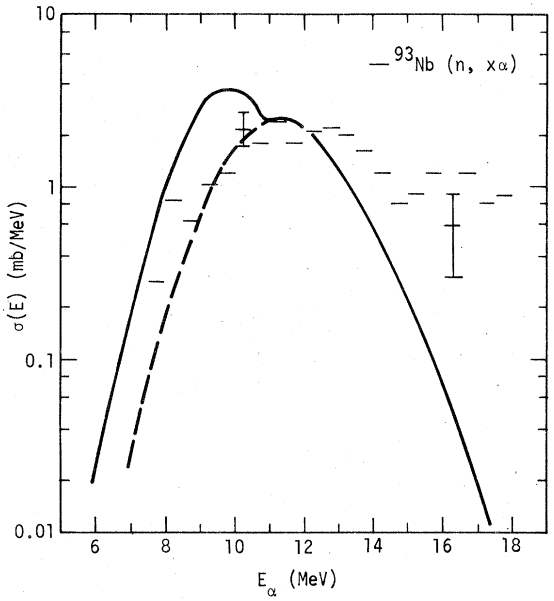

FIG. 6. Same as Fig. 3 for the $^{93}Nb(n,x\alpha)$ reaction.

IV. DISCUSSION

These results can be compared with other measurements, also listed in the table where the charged particles were detected directly and with activation measurements. Colli *et al.*[3] measured the protons at an average laboratory angle of 15° from 14-MeV neutron bombardment of ^{51}V. Their differential cross section can be multiplied by 4π to give the total proton production cross section if the angular distribution is isotropic. Most likely, however, the angular distribution is forward peaked and this procedure will give an overestimate of the cross section. The compensating factor is that protons below about 3 MeV were not observed in Ref. 3. By chance, these factors com-

TABLE I. Proton, deuteron, and α-particle production cross sections by 15-MeV neutrons.

	This work	Previous work	Activation
$^{51}V(n,xp)$	91 ± 14	87[a]	>31[b]
$^{51}V(n,xd)$	7 ± 3	···	···
$^{51}V(n,x\alpha)$	17 ± 3	···	19.5 ± 1.2[b]
$^{93}Nb(n,xp)$	51 ± 8	>22 ± 8[c]	···
$^{93}Nb(n,xd)$	8 ± 3	···	···
$^{93}Nb(n,x\alpha)$	14 ± 3	9.5 ± 1.4[d]	>11.7[e]

[a] Reference 3 at 14 MeV, $(d\sigma/d\Omega)(\theta=15°)\times 4\pi$.
[b] Reference 4 at 14.78 MeV.
[c] Protons above 6.5 MeV only, Ref. 7 at $E_n=14$ MeV.
[d] Reference 7 at 14.2 MeV.
[e] Sum of $\sigma(n,\alpha)=9.2$ mb (Ref. 9) and $\sigma(n,n'\alpha)$ to isomeric state $=2.5\pm1.1$ mb at 14.7 MeV (Ref. 10).

pensate very well and good agreement obtains with the present result.

The cross section of $^{51}V(n, p)^{51}Ti$ measured by activation techniques[4] gives a lower limit or the total proton production cross section. This limit is consistent with the present result. For the $^{51}V(n, x\alpha)$ reactions, all the residual nuclei can be measured by activation. The $^{51}V(n, n\alpha + \alpha n)^{47}Sc$ cross section was reported[5] to be less than 0.3 mb at 14.5 MeV. If we assume that it is similarly small at 15 MeV, then the total $^{51}V(n, x\alpha)$ cross section is essentially that of $^{51}V(n, \alpha)^{48}Sc$, or 19.5 ± 1.2 mb[4] which is consistent with our present results.

For the $^{93}Nb(n, xp)$ cross section, a value of 22 ± 8 mb was reported[6] for protons above 6.5 MeV. That portion of our proton spectrum gives 29 ± 4 mb, in agreement within the errors. For the $^{93}Nb(n, x\alpha)$ cross section, Bormann *et al.*[7] report 9.5 ± 1.4 mb at 14.2 MeV. This value is slightly less than the present 14 ± 3 mb although the error bars nearly touch. The difference in incident neutron energy could account for this small discrepancy. Kulisic *et al.*[8] report 9.3 ± 2.8 mb at 14.7 MeV in reasonable agreement with the present result.

Activation data give a lower limit for the $^{93}Nb(n, x\alpha)$ cross section. For $^{93}Nb(n, \alpha)^{90}Y$ the many cross section data have been evaluated[9] to be 9.2 mb. For $^{93}Nb(n, n\alpha + \alpha n)^{89}Y^m$ the cross section has been measured at 14.7 MeV to be 2.5 ± 1.1 mb.[10] The missing part is the $^{93}Nb(n, n\alpha + \alpha n)^{89}Y^g$ cross section. The lower limit is then about 11.7 mb and is consistent with the presently measured value of 14 ± 3 mb. We conclude that the $^{93}Nb(n, n\alpha + \alpha n)^{89}Y^g$ cross section is 2^{+3}_{-2} mb.

These measurements contrast significantly with those reported in Ref. 1. Both ^{51}V and ^{93}Nb have neutron separation energies which exceed the proton separation energies by about 3 MeV. In neither case does the $(n, n'p)$ cross section approach the 300 mb observed[1] for ^{46}Ti, for which the neutron-proton separation energy difference is also 3 MeV. The reduction for Nb is expected because of the larger Coulomb barrier for this nucleus, but the corresponding barriers for Ti and V are nearly equal.

In an effort to understand this difference, Hauser-Feshbach calculations of the proton and α-particle spectra for 15-MeV neutron bombardment of ^{46}Ti, ^{51}V, and ^{93}Nb were performed. Details of the computer code used have already been published,[11] but the code was modified to include the γ-ray decay channel.

Transmission coefficients for protons and α particles were calculated from the optical potentials proposed by Becchetti and Greenlees[12] and Huizenga and Igo,[13] respectively. Neutron transmission coefficients were calculated with the optical parameters of Becchetti and Greenlees,[12] Wilmore and Hodgson,[14] and Holmquist and Wiedling.[15] The potential of Ref. 14 predicted the highest absorption cross sections at low energies, while that of Ref. 12 yielded the highest values near 15 MeV. Comparison of measured total and nonelastic neutron cross sections for V and Nb with the predictions showed that the Holmquist and Wiedling potential provided the best fit for V and the Wilmore and Hodgson potential the best fit for Nb. It is interesting that the percentage discrepancies in matching the total and the nonelastic cross sections were quite similar, suggesting that although these potentials were derived principally from elastic scattering data, the predicted elastic cross sections vary over a range of as much as 15% at some energies. The potentials of Refs. 14 and 15 were used to calculate the transmission coefficients for neutrons on V and Nb, respectively.

γ-ray transmission coefficients were based on the formulas proposed by Woosley *et al.*[16] These authors utilize a giant dipole form for the $E1$ strength and assume that the $M1$ transmission coefficient has a form given by a single particle model, $T(M1) = cE_\gamma^3$. The constant c relating $T(M1)$ to E_γ^3 has been determined empirically by these authors[8] to be 1.95×10^{-8}. The $E1$ transmission coefficient has the form

$$T_{E1}^{(\epsilon)} = 1.3 \times 10^{-6} A_c \frac{\Gamma_{GDR}\,\epsilon^4}{(\epsilon^2 - \epsilon_{GDR}^2)^2 + (\Gamma_{GDR}\,\epsilon)^2},$$

where A_c is the mass number of the compound nucleus, Γ_{GDR} and ϵ_{GDR} are the width and location of the giant electric dipole resonance, and ϵ is the energy of the γ ray emitted. The authors of Ref. 8 propose values of $35/A_c^{1/6}$ MeV and $33/A_c^{1/3}$ MeV for ϵ_{GDR} and Γ_{GDR}, respectively, and these were used in the present calculations.

Level density parameters for the residual nuclei were based on calculations with a computer code which calculates[11] level densities from specific single particle schemes using a thermodynamic formalism.[17] These values were then modified slightly (if necessary) to achieve fits to the low energy portions of the proton and α spectra. Calculations were carried out for ^{51}V and ^{93}Nb as well as ^{46}Ti, since for the latter nucleus the calculations reported in Ref. 1 did not include the γ-ray decay channel. Level density parameters used are listed in Table II.

The resulting calculations provide a fairly good fit to the data, as can be seen in Figs. 3–8. In particular, the large difference between the size of the $(n, n'p)$ contribution to the $^{46}Ti(n, xp)$ spectrum compared to $^{51}V(n, xp)$ is consistent with cal-

TABLE II. Level schemes including approximately 10 levels were used for each nucleus at low excitation energy, with the Fermi gas form used at higher energies.

Nucleus	Level density parameters[a] a	δ	Nucleus	Level density parameters[a] a	δ
^{47}Ti	5.9	0	^{50}Sc	6.2	−1.0
^{46}Ti	5.85	1.4	^{48}Sc	5.9	−1.6
^{46}Sc	5.85	−1.4	^{47}Sc	5.9	0
^{45}Ti	5.8	0	^{47}Ca	5.9	0
^{45}Sc	5.8	0	^{94}Nb	11.7	−0.5
^{45}Ca	5.8	0	^{93}Nb	11.7	0.55
^{43}Ca	5.5	−0.2	^{93}Zr	11.7	0.25
^{42}Ca	5.5	1.2	^{92}Nb	11.6	−0.5
^{42}K	5.5	−1.6	^{92}Zr	11.6	1.6
^{52}V	6.3	−1.0	^{92}Y	11.6	−5
^{51}V	6.3	0.4	^{90}Y	11.4	0.35
^{51}Ti	6.3	0.6	^{89}Y	11.4	−0.6
^{50}V	6.2	−1.0	^{89}Sr	11.4	−0.6
^{50}Ti	6.2	1.8			

[a] The a and δ are the parameters of the traditional Fermi gas form

$$\rho(u)=\frac{\sqrt{\pi}\exp\{2[a(u-\delta)]^{1/2}\}}{12a^{1/4}(u-\delta)^{5/4}}.$$

culations.

The data do not yield values for $\sigma(n, p)$ and $\sigma(n, n'p)$ directly, but these two reactions are expected to have sufficiently different spectral shapes that a calculation which fits the lowest 9 MeV of the charged particle spectrum provides a good estimate of the relative contributions of these two reactions. Emission spectra from (n, p) reactions are expected to fall rapidly for energies below the Coulomb barrier, while $(n, n'p)$ reactions will produce proton spectra which are significant below the Coulomb barrier [if the Q value for $(n, 2n)$ is more negative than that for $(n, n'p)$] but will fall off at higher energies where the $(n, 2n)$ reaction may occur.

Based on the calculations shown in the figures, the magnitude of the $(n, n'p)$ cross section is about a factor of 6 larger for ^{46}Ti than for ^{51}V. As mentioned previously, the neutron and proton binding energies differ by about the same amount (~3 MeV) in both nuclei and the Coulomb barriers for the two nuclei are similar.

Closer examination of the parameters which enter the calculation shows that other factors play an important role in determining the $\sigma(n, n'p)$ cross section. First, not only the difference $B_n - B_p$ but also the absolute magnitudes of these quantities affect the $(n, n'p)$ cross section. For ^{46}Ti, B_n and B_p are 13.2 and 10.35 MeV, respectively, while for ^{51}V the corresponding binding energies are 11.04 and 8.04 MeV. The larger magnitudes of these quantities for ^{46}Ti shift the outgoing neutron energy for an (n, n') reaction which leads to an $(n, n'p)$ reaction down from the range 4 to 7 MeV (for ^{51}V to 1.8 to 4.65 MeV (for ^{46}Ti) if 15-MeV neutrons are incident on the target; this change moves the "window" for such reactions closer to the peak (between 1 and 2 MeV) in the neutron evaporation spectrum. A trial calculation for ^{51}V showed that changing the B_n and B_p values to those of ^{46}Ti increased the $(n, n'p)$ cross section by about

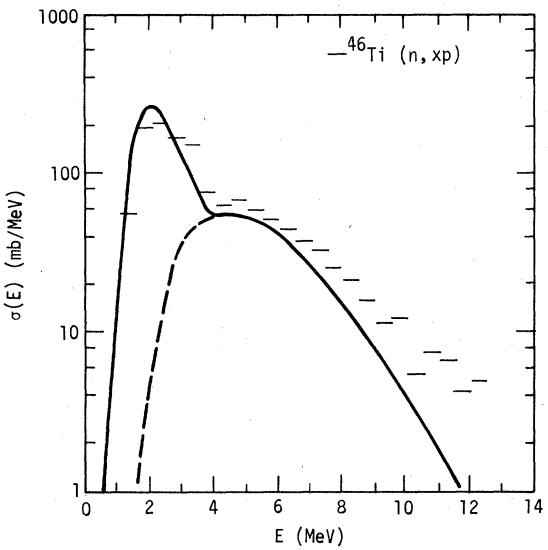

FIG. 7. Same as Fig. 3 for the ^{46}Ti(n, xp) reaction. Data are from Ref. 1.

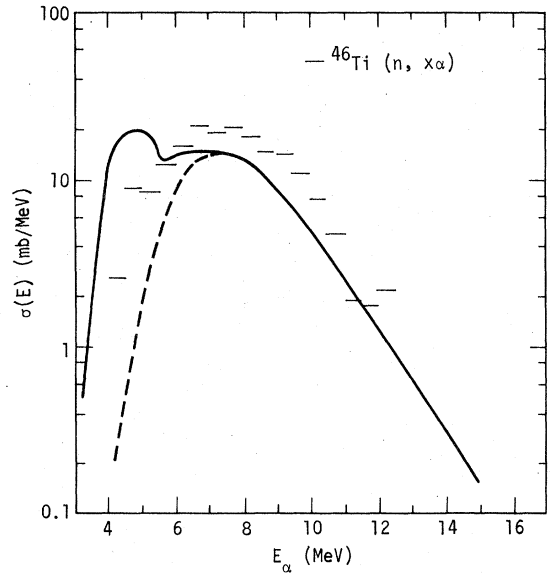

FIG. 8. Same as Fig. 3 for the ^{46}Ti$(n, x\alpha)$ reaction. Data are from Ref. 1.

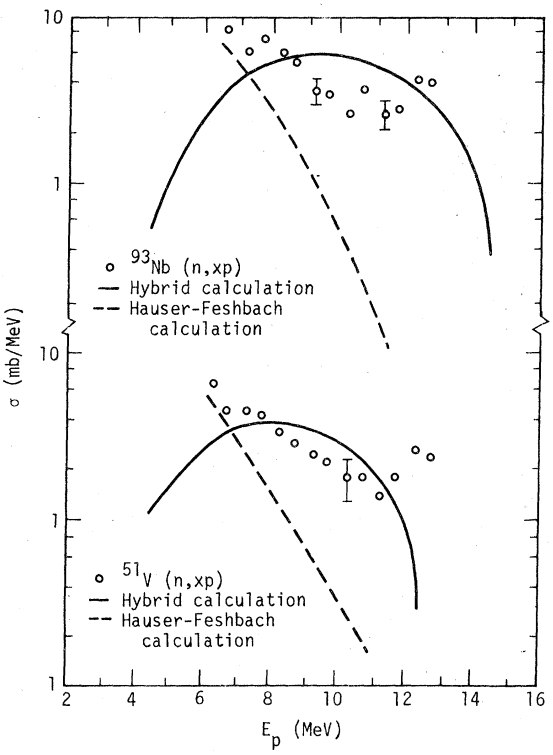

FIG. 9. Comparison of the highest energy portions of the $^{51}V(n,xp)$ and $^{93}Nb(n,xp)$ spectra with predictions of the hybrid model (solid line). The statistical prediction is shown for comparison (dashed line).

10%.

This factor is much smaller than the population difference of the corresponding (n, n') residual excitation region would suggest. The fact that the average neutron emission energy for an $(n, n'p)$ reaction is reduced by this change means that the average angular momentum removed by the neutron decreases. As a result, the angular momentum distribution for states populated by (n, n') reactions narrows, and a relatively smaller fraction of flux in low angular momentum levels results. Thus, although the population of levels in the energy window is increased, the relative probability for proton decay is reduced, because of a lack of low-lying levels of high spin in ^{50}Ti.

A second difference between the two targets is that one is even in A and the other odd in A. The $(n, n'p)$ reaction on ^{51}V leads to ^{50}Ti, an even-even nucleus with a low level density at low excitation energies. Not only are there only three levels in the first 3 MeV of excitation energy but these are also all of positive parity. In contrast, the $(n, n'p)$ reaction on ^{46}Ti leads to ^{45}Sc, a nuclide with nine levels in the lowest MeV of excitation including some of each parity. Thus, if sub-Coulomb barrier decays occur primarily through $l = 0$ proton emission, levels with a much larger range of J values and with both parities in the target nucleus can decay through such a process for ^{46}Ti, in contrast to ^{51}V. Again, repeating the calculation for ^{51}V using the levels of ^{45}Sc (adjusted by $\frac{1}{2}$ in the spin) instead of those for ^{50}Ti increased the $(n, n'p)$ cross section by almost a factor of 3.

An additional difference between ^{46}Ti and ^{51}V is that the ground state spin of the former is 0 and that of the latter is $\frac{7}{2}$. This results in a somewhat larger average spin of the compound nucleus ^{52}V than that for ^{47}Ti and a slightly different spin distribution after the (n, n') reaction. According to the calculation, the difference in target spin causes about a 20% change in the $(n, n'p)$ cross section.

The fact that no one of these factors accounts entirely for the large difference between the $(n, n'p)$ cross section of ^{51}V and ^{46}Ti suggests that the factors may be coupled. The effect of shifting the binding energy values of ^{51}V to those of ^{46}Ti was found to be about 10% if no other parameters were changed; if the final levels of ^{50}Ti are replaced by those of ^{45}Sc, the change caused by modifying binding energies becomes about 45%. Target spin effects are similarly enhanced by the binding energy change. All of these effects are related to the proton to γ-ray width ratios as a function of the angular momentum of the level. Substituting levels of large spin in the final nucleus for the few levels of low spin in ^{50}Ti allows states with larger J values to proton decay rather than γ-ray decay; this is coupled to changes in average spin of levels populated in an (n,n') reaction produced by changes in (1) binding energy (i.e., average neutron emission energy in the region of interest) and (2) target spin. These factors[18] would tend to have a similar correlation in comparing other odd-A–odd-Z with even-A targets; thus, a general reduction of the importance of the $(n,n'p)$ reaction would be expected for odd-A–odd-Z targets relative to even-A–even-Z targets in a given mass region.

The comparisons shown in Figs. 3–6 show evidence for a nonequilibrium component in the charged-particle data. In Fig. 9 a comparison is presented of the high energy parts of the $^{51}V(n,xp)$ and $^{93}Nb(n,xp)$ spectra with those predicted by the hybrid model for preequilibrium reactions. This model has been developed by Blann[19] and the computer code used in making the calculations has been described previously.[20]

Calculations for both targets are larger than the data and show less structure. Both of these characteristics may be due to the fact that the targets are both near closed shells. As has been pointed out in Ref. 20, comparison of (p,n) spectra for targets near or at closed shells[21] with those more removed from closed shells[20] shows considerably

more structure for the former. In addition, the magnitude of the preequilibrium portion of the spectrum may also be reduced by shell effects, since the density of neutron-particle–proton-hole states would be reduced at low excitation energies for closed shell nuclei. The calculations shown in Fig. 9 are based on global densities for such states and thus do not incorporate shell effects.

V. SUMMARY

Charged particle production cross sections have been measured for 15-MeV neutrons incident on ^{51}V and ^{93}Nb. As was found in a previous study of the targets ^{27}Al, ^{46}Ti, and ^{48}Ti, the largest cross sections are for protons with α and deuteron cross sections smaller by factors of about 3 and 6, respectively. A significant fraction of the proton cross section results from $(n, n'p)$ reactions in targets where this threshold is lower than that for $(n, 2n)$. For the targets investigated to date, the $(n, n'\alpha)$ reaction is much less important in producing α particles than the $(n, n'p)$ reaction is for protons. The consistently small (n, d) cross sections are apparently the result of the very small statistical cross section for this reaction, in contrast to (n, p) and (n, α); the shape of the (n, d) spectra in emission energy and angle suggest that this cross section is due in large part to nonstatistical reactions.

---

†Work performed under the auspices of the U.S. Energy Research and Development Administration, W-7405-Eng-48.

[1]S. M. Grimes, R. C. Haight, and J. D. Anderson, Nucl. Sci. Eng. 62, 187 (1977).

[2]R. C. Haight, S. M. Grimes, B. J. Tuckey, and J. D. Anderson, Lawrence Livermore Laboratory Report No. UCRL 77151 (unpublished).

[3]L. Colli, I. Iori, S. Micheletti, and M. Pignanelli, Nuovo Cimento 21, 966 (1961).

[4]J. C. Robertson, B. Audric, and P. Kolkowski, J. Nucl. Energy 27, 531 (1973).

[5]M. Hillman, Phys. Rev. 129, 2227 (1963).

[6]V. V. Verbinski, T. Hurlimann, W. E. Stephens, and E. J. Winhold, Phys. Rev. 108, 779 (1957).

[7]M. Bormann, W. Schmidt, V. Schröder, W. Scobel, and U. Seebeck, Nucl. Phys. A186, 65 (1972).

[8]P. Kulisic, V. Ajdacic, N. Cindro, B. Lalovic, and P. Strohal, Nucl. Phys. 54, 17 (1964).

[9]R. Howerton, A. Smith, P. Guenther, and J. Whalen, Argonne National Laboratory Report No. ANL/NDM-6, 1974 (unpublished).

[10]E. T. Bramlitt and R. W. Fink, Phys. Rev. 131, 2649 (1963).

[11]S. M. Grimes, J. D. Anderson, J. W. McClure, B. A. Pohl, and C. Wong, Phys. Rev. C 10, 2373 (1974).

[12]F. D. Becchetti and G. W. Greenlees, Phys. Rev. 182, 1190 (1969).

[13]J. R. Huizenga and G. J. Igo, Nucl. Phys. 29, 462 (1962).

[14]D. Wilmore and P. Hodgson, Nucl. Phys. 55, 673 (1964).

[15]B. Holmquist and F. Wiedling, J. Nucl. Energy 27, 543 (1973).

[16]S. E. Woosley, W. A. Fowler, J. A. Holmes, and B. A. Zimmerman, California Inst. of Technology Report No. OAP-422, 1976 (unpublished).

[17]L. G. Moretto, Nucl. Phys. A182, 641 (1972).

[18]The correlation of target spin and number of final levels at low excitation in the residual nucleus with even-A or odd-A–odd-Z will depend on shell structure. In a region near a closed shell, the odd-A–odd-Z nucleus reached by an $(n,n'p)$ reaction on an even-A target might not have a large number of low-lying levels and, similarly, the target spin of the odd-A nucleus could be $\frac{1}{2}$, which is only slightly larger than the 0 spin expected for even A. Finally, nucleon binding energies for even-A targets tend to be larger than those for odd-A–odd-Z targets because of pairing effects, but this could also be reduced by shell effects.

[19]M. Blann, Phys. Rev. Lett. 27, 337 (1971); 28, 757 (1972); Nucl. Phys. A213, 570 (1973).

[20]S. M. Grimes, J. D. Anderson, and C. Wong, Phys. Rev. C 13, 2224 (1976).

[21]M. Blann, R. R. Doering, A. Galonsky, D. M. Patterson, and F. E. Serr, Nucl. Phys. A257, 15 (1976).